

# Rotational aerophones

N. H. Fletcher<sup>a)</sup>

Research School of Physical Sciences and Engineering, Australian National University, Canberra 0200, Australia

A. Z. Tarnopolsky and J. C. S. Lai

School of Aerospace and Mechanical Engineering, University College, University of New South Wales, Australian Defence Force Academy, Canberra 2600, Australia

(Received 11 September 2001; accepted for publication 29 November 2001)

Free rotational aerophones such as the bullroarer, which consists of a wooden slat whirled around on the end of a string, and which emits a loud pulsating roar, have been used in many ancient and traditional societies for ceremonial purposes. This article presents an experimental and theoretical investigation of this instrument. The aerodynamics of rotational behavior is elucidated, and relates slat rotation frequency to slat width and velocity through the air. Analysis shows that sound production is due to generation of an oscillating-rotating dipole across the slat, the role of the vortices shed by the slat being relatively minor. Apparent discrepancies between the behavior of a bullroarer slat and a slat mounted on an axle in a wind tunnel are shown to be due to viscous friction in the bearings of the wind-tunnel experiment. © 2002 Acoustical Society of America. [DOI: 10.1121/1.1446053]

PACS numbers: 43.28.Ra, 43.75.-z [MSH]

## I. INTRODUCTION

The device generally called a “bullroarer” has an important place in many cultures,<sup>1</sup> ranging from predynastic Egypt of 3000 BC and the ancient tribal traditions of the Australian Aboriginal people, to the Inuit of Northern Canada. It consists simply of a thin slat of wood, typically 200–400 mm long, 30–60 mm wide and 5–10 mm thick, pierced with a small hole at one end through which is passed a thin cord about 1 m long, by means of which it is whirled in circles by the player. The slat may be simply rectangular and unadorned, or may have a more complex shape and be decorated with paintings of tribal gods or totems. An Australian example, the name of which is secret-sacred in Aboriginal languages, is shown in Fig. 1. The cross-section of this bullroarer is trapezoidal, as is common, rather than simply rectangular. During the whirling motion, the slat rotates about its long axis, producing a loud growling roar which pulsates at the rate of rotation, about 1 to 1.5 Hz, and also at about twice this rate. It is interesting that the frequency of the bullroarer drone is about 70 Hz, which is comparable with the frequency of the drone of the lip-blown didjeridu,<sup>2</sup> also used in ceremonies. One might feel with Marcuse<sup>1</sup> that bullroarers are not really musical instruments, but the bullroarer has in fact been used in at least one piece of classical music—the ballet Suite *Corroboree* by Australian composer John Antill<sup>3</sup>—to evoke the spirit of the Aboriginal people. We may term these devices “free rotational aerophones” and their investigation is the main subject of this article.

## II. FREE AEROPHONE EXPERIMENTS

In an initial study, the bullroarer of Fig. 1 was whirled around in a vertical plane, as shown in Fig. 2, using a string

of length about 70 cm, and an audio recording was made, along with a video record for later frame-by-frame analysis. At very low arm rotation speeds A or B, axial rotation C of the slat did not occur, but this began for arm rotation speeds of around 30 rpm (0.5 Hz) and was fully developed at the normal arm rotation speed of about 60–90 rpm (1–1.5 Hz). The pulsations synchronous with the hand motion are presumably associated with variations in the speed of rotation of the slat caused by uneven motion of the player’s arm. The player’s hand motion was generally elliptical, but the path of the slat was quite closely circular, with a radius of about 70 cm for slow arm motion and 80 cm for rapid rotation. The angular position of the slat in its orbit trailed that of the hand by an angle  $\phi$  as shown in the second panel of Fig. 2. The variation of this trailing angle during one arm revolution is shown in Fig. 3. The angle  $\phi$  increased with increased speed of arm rotation and oscillated quasi-periodically at twice the arm rotation speed, as might be expected from the relationship between circular slat motion and elliptical arm motion. The varying angle between the long axis of the slat and its direction of translational motion presumably contributes to sound pulsations.

In normal playing, the string linking the slat of the bullroarer to the player’s hand traces out a conical surface with an apical semi-angle of about 80 degrees. In quasi-steady operation, the bullroarer rotates in one direction, C, about its axis for several seconds, then stops and reverses its motion, the orientation of the cone swept out by the string reversing simultaneously. This rotation reversal is clearly associated with progressive twisting of the string and depends upon its length and thickness, while the cone-axis reversal is apparently associated with a lift force, the direction of which depends upon the sense of the axial rotation, as for a rotating cylinder.<sup>4</sup>

In one set of experiments in an anechoic chamber, the

<sup>a)</sup>Electronic mail: neville.fletcher@anu.edu.au

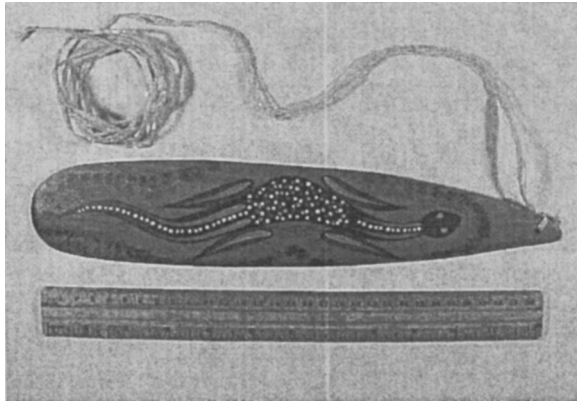


FIG. 1. A bullroarer, from Northern Australia. The ochre-painted design indicates the “dreaming” or totem of the maker.

microphone was positioned on the rotation axis and at a distance of about 1 m from the plane of rotation while the bullroarer was whirled at about 90 rpm (1.5 Hz). Figure 4(a) shows the signal recorded over a time of about 0.6 s. The generally sinusoidal waveform, with a frequency of about 70 Hz, is modulated at about 3 Hz in synchrony with the arm rotation. Because of the twofold rotation symmetry of the slat, the axial rotation speed is just half the acoustic frequency, and therefore about 35 Hz or 2100 rpm. The modulation depth and maximum sound output are both slightly different for the two senses of axial rotation of the slat, an effect presumably associated with its trapezoidal cross-section.

Figure 4(b) shows the spectrum of the radiated sound. It consists essentially of a single component at about 70 Hz, the width of the peak presumably being due to aerodynamic unsteadiness in frequency and to the amplitude variations shown in Fig. 4(a). The level of the second harmonic is about  $-30$  dB relative to the fundamental, and the general noise level is low.

Because the genuine bullroarer slat is complicated geometrically, it was desirable to replace this by a simpler slat for more detailed analysis. Experiments similar to those carried out on the bullroarer were therefore performed using a simple rectangular slat of aluminum, 335 mm long, 40 mm wide and 1 mm thick, whirled by hand on a string of length 70 cm. The behavior was generally similar to that of the bullroarer except that the slat did not begin rotation spontaneously and had to be twisted initially. The instrument pro-

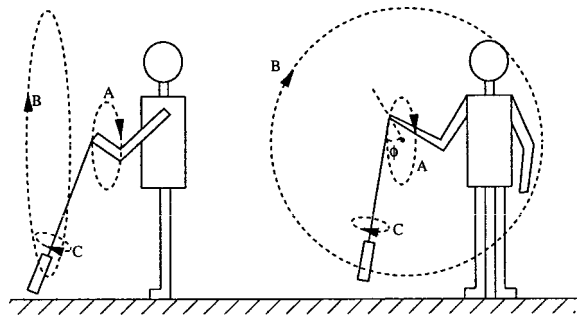


FIG. 2. Playing the bullroarer, with the rotational motions and the trailing angle  $\phi$  defined. The string describes a conical path with apex directed successively towards and away from the player.

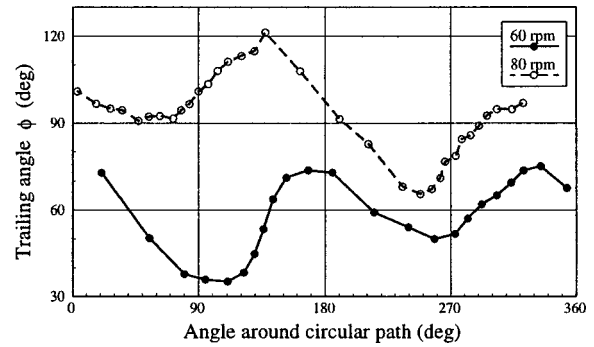


FIG. 3. Variation of the trailing angle  $\phi$  between the projection of the player’s arm on the rotation plane and the string direction, during one cycle of revolution. Measurements for two arm rotation rates are shown.

duced the same pulsating drone, and the sound spectrum and total radiated power were both also similar. The radiation pattern, measured in an open environment, was essentially isotropic to within about  $\pm 3$  dB, more accurate measurement being impossible because of variation in the sound signal.

The measured dependence of the rotation rate  $f$  or angular rotation rate  $\omega = 2\pi f$  of the slat (half the sound frequency, because of the twofold symmetry of the slat) on arm rotation rate  $F$  or angular rate  $\Omega = 2\pi F$ , for slats of several widths, is shown in Fig. 5. As shown in the figure, the drone frequency is approximately proportional to the arm rotation rate and thus to the translational speed  $V$  of the centroid of the slat through the air, and approximately inversely proportional to the slat width  $W$ . The more precise result derived from the experimental regressions for a 70-cm string length is

$$\omega \approx 0.4\Omega^{0.9}W^{-1.3} \approx 0.5V^{0.9}W^{-1.3} \quad (1)$$

with an uncertainty of about  $\pm 0.2$  in the values of the exponents and of about  $\pm 20\%$  in the value of the multiplying constant, which depends upon the length of the string. The equivalent range of airspeed  $V$  over which this relation was established was about  $5 - 10 \text{ m s}^{-1}$ .

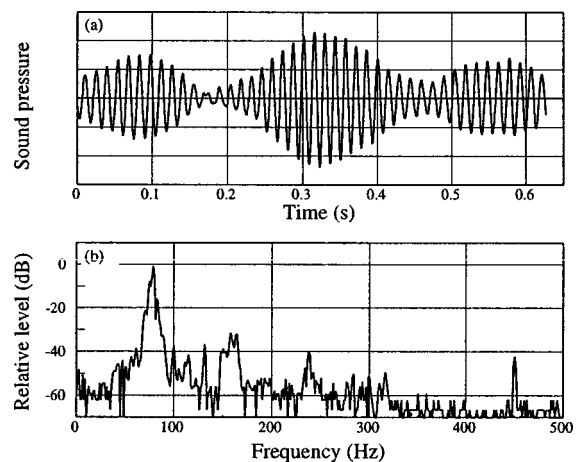


FIG. 4. (a) Pressure waveform of the sound produced by a bullroarer rotating at about 90 rpm. The sound frequency is about 70 Hz and the frequency of the pulsations about 3 Hz. The pulsations are more prominent for one direction of slat rotation than for the other. (b) Spectral analysis of the quasi-steady sound, which differs little for the two rotation directions.

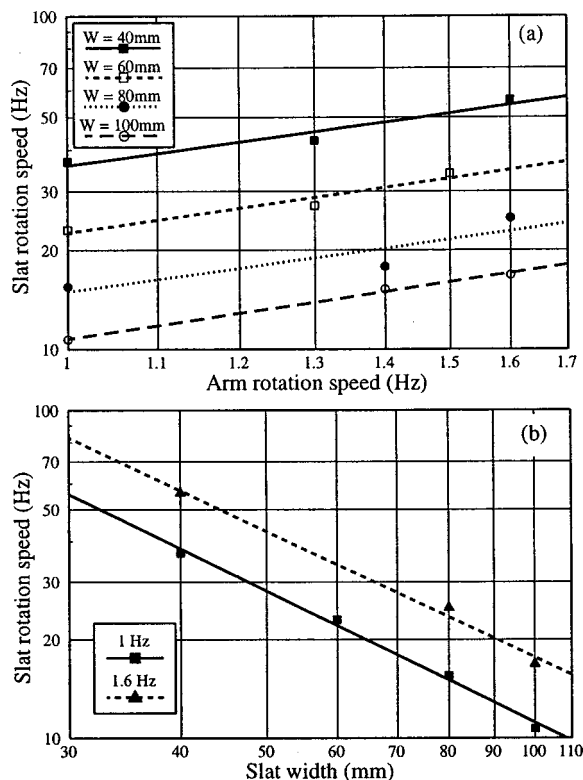


FIG. 5. Slat rotation speed  $f$  as a function of (a) arm rotation speed  $F$ , and (b) slat width  $W$ , for a hand-whirled slat on a string of length 70 cm.

An alternative analysis of the experimental data can be carried out by plotting  $f$  against  $F/W$ , as is suggested by later theory. The result, plotted in Fig. 6, gives a regression of the form

$$f \approx 1.6F/W - 5 \quad \text{or} \quad \omega \approx 1.6\Omega/W - 30 \quad (2)$$

for a string length of 70 cm. This expression can be rewritten more generally as

$$\omega \approx 1.1V/W - 30. \quad (3)$$

It is perhaps significant to note that the rotation speed is such that the edge of the slat is moving at about half the speed of the airstream.

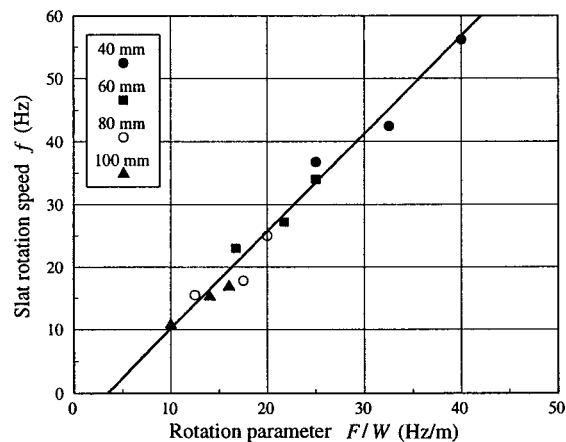


FIG. 6. Slat rotation speed  $f$  as a function of  $F/W$  for a slat of width  $W$  whirled at frequency  $F$  on a string of length 70 cm.

Because the available anechoic chamber was small and had a cut-off frequency above 100 Hz, which is well above the sound frequencies involved, it was necessary to perform acoustic measurements at an outdoor site, actually the middle of an isolated sports oval. Particular interest attaches to the radiated sound power and its dependence upon slat width and arm rotation speed. The measurements are complicated by the sound pulsations and by the slower rise and fall of sound level as the string is untwisted and then retwisted. There is, however, a plateau level in each long cycle during which fairly reliable measurement is possible.

Measurements were made using four rectangular aluminum slats 335 mm long and 1 mm thick, and ranging in width between 40 and 100 mm. The slats were whirled by hand using a string 70 cm in length. Sound pressure measurements were made on the rotation axis direction at a distance of 4 m from the player, this distance being dictated by the balance between sound output and ambient noise. Since the sound frequency in the experiments was in the range 40–160 Hz, this distance is less than the sound wavelength in some cases, and near-field effects must be considered. The pressure amplitude of a dipole, measured at distance  $r$ , exceeds the radiation contribution at this distance by a factor  $[1 + (jkr)^{-1}]$ , where  $k = 2\pi/\lambda$  and  $\lambda$  is the sound wavelength.<sup>5</sup> Converting this to a sound pressure level, however, shows that the maximum correction is less than 1.3 dB, which is not significant in our measurements.

The “linear” setting (no frequency weighting) on a sound level meter with real-time  $\frac{1}{3}$  octave frequency analysis was used, a spectral display being necessary in order to discriminate against wind noise and other environmental noise at these low frequencies. The results showed that the radiated sound level was completely independent of slat width over the width range tested and at arm rotation rates between 72 and 120 rpm ( $7.5 < \Omega < 12.6 \text{ s}^{-1}$  or  $6 < V < 10 \text{ m s}^{-1}$ ). The sound pressure level at the measuring position was 60 dB at 72 rpm and 72 dB at 120 rpm with an uncertainty of about  $\pm 1$  dB in each case.

A further measurement in which the player turned sequentially through 45-degree angles established that the radiation pattern was uniform to within an uncertainty of about  $\pm 1$  dB so that the SPL values can be converted to radiated acoustic power. Assuming good reflection at these frequencies from the grass field surface, this gives a radiated power of about 1 mW at an arm rotation speed of 120 rpm and about 60  $\mu$ W at 72 rpm. The approximate behavior of radiated sound power was thus

$$P = \text{const} \times \Omega^{5.4}. \quad (4)$$

There is no dependence upon  $W$  and an uncertainty of perhaps  $\pm 1$  in the exponent. Since the sound source, being slaved to the rotation of the slat, is coherent along its length which is much smaller than the sound wavelength, we expect that the radiated power should be proportional to the square of slat length  $H$ , but this dependence was not examined experimentally.

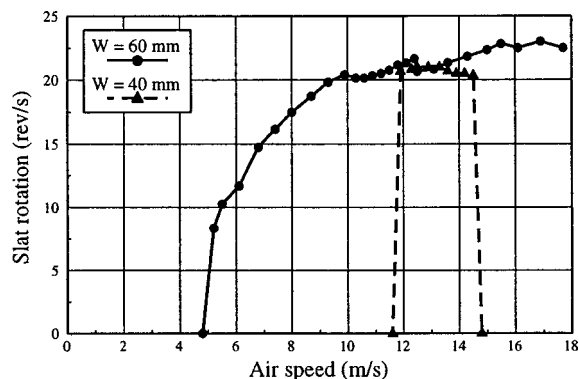


FIG. 7. Measured rotational frequency of the 60-mm slat as a function of airspeed in the wind tunnel. Also shown is the measured behavior of a 40-mm slat, which has a very limited range of airspeeds for rotation.

### III. WIND-TUNNEL EXPERIMENTS

A fundamental question to emerge is that of the mechanism controlling the axial rotation of the slat. This was therefore investigated in a series of carefully controlled experiments in a wind tunnel. For this study, a simple rectangular steel slat 253 mm long, 1.5 mm thick and 20, 40 or 60 mm wide was mounted on Teflon bearings by means of an axle passing along its centerline. The bearings were lubricated with a light oil. The wind-tunnel cross-section was  $255 \times 255 \text{ mm}^2$  and the length of the slat extended almost completely across the width of the tunnel, so that there was a good approximation to two-dimensional unbounded flow. The air speed in the wind tunnel was measured using a pitot tube connected to a micro manometer, and the slat rotation speed was measured using an optical tachometer on the axle. The maximum attainable air speed was  $18 \text{ m s}^{-1}$ .

The following conclusions were readily established experimentally:

- (1) The slat will not generally begin rotation spontaneously under the influence of air flow, but requires to have an initial rotation imparted to it. Depending upon the airspeed, the slat rotation may then either settle down to a steady value or else stop.
- (2) For any slat, there is a minimum air flow velocity below which rotation cannot be maintained. This critical velocity increases as the width of the slat is decreased. (In the experiment, it was impossible to maintain rotation of the 20-mm slat under any attainable air speed.)
- (3) At least in the case of the 40-mm slat, there is also a maximum air flow velocity above which rotation cannot be maintained. No such upper limit was found for the wider slat up to the attainable wind tunnel air speed.
- (4) The steady rotation frequency does not depend greatly upon the width of the slat in the two cases studied, and increases towards saturation with increasing air speed.

The experimental basis for these conclusions is demonstrated in Fig. 7. There are several features of the wind-tunnel experiments that are in conflict with observations on the bullroarer in normal operation. The first is the fact that the rotation speed of the 60-mm slat in the wind tunnel apparently reaches a plateau value once the airspeed exceeds

about  $10 \text{ m s}^{-1}$ , while the bullroarer rotation speed continues to increase about linearly with airspeed in the range 6 to  $12 \text{ m s}^{-1}$ , as shown in Fig. 5 and Eq. (1). The second is that the 40-mm slat will rotate over only a limited airspeed range and ceases rotation if the airspeed is too high. Finally, the rotation speeds of the 40- and 60-mm slats are nearly the same in the airspeed range in which both rotate. The slats used for these determinations were very similar to those used in the free-aerophone experiments except for the mass, which should not be significant in wind-tunnel measurements. An explanation for these discrepancies must be sought, and is given in the next section.

### IV. SIMPLE THEORY

This investigation scarcely warrants development of a detailed aerodynamic study, which would be a complex operation indeed. Fortunately it is straightforward to devise a simple theory that explains the experimental findings, at least in a semi-quantitative manner. A simple theory also exposes the physical principles involved in a more accessible way.

Consider a thin slat of width  $W$ , mounted as in the wind-tunnel experiment and rotating with angular velocity  $\omega$  in an air flow of speed  $V$ . This assumption can later be specialized to apply to the cord-supported slat. The total torque acting on the slat can be divided conceptually into three parts, although it is not really possible to separate these rigorously because of the nonlinear nature of aerodynamic forces. First, there is the aerodynamic drag torque  $\Gamma_1$  per unit length of slat arising from the rotation. On the assumption that this torque is proportional to the product of the square of the slat-edge velocity  $W\omega/2$ , the slat area per unit length  $W$ , and the slat radius of gyration  $W/12^{1/2}$ , this can be written to a first approximation as

$$\Gamma_1 \approx -\alpha \rho W^4 \omega^2, \quad (5)$$

where  $\rho$  is the density of air and  $\alpha$  is a nondimensional constant.

Second, the frictional torque in the bearings must be taken into account. This torque depends upon the load borne by the bearings, which is largely the aerodynamic drag created by the interaction of the airstream with the rotating slat. While this varies periodically through the rotation as the angle of incidence changes, its average value is proportional to  $\rho V^2 W$  per unit length. For generality the bearing torque should include a velocity-independent contribution from dry friction, a viscous friction contribution that is proportional to slat rotation speed, and a residual friction independent of the aerodynamic load. It is a reasonable approximation to assume that both the dry friction and the viscous friction are proportional to the total load on the bearings, and the resulting torque is also proportional to bearing radius  $r$ , so that the total bearing torque  $\Gamma_2$  per unit length of slat can be written as

$$\Gamma_2 = -\Gamma_0 - \rho W r V^2 (\beta + \beta' \omega), \quad (6)$$

where  $\Gamma_0$  is the frictional torque of the bearing under zero airflow conditions,  $\beta$  is a nondimensional constant, and  $\beta'$  is a constant with the dimensions of time.

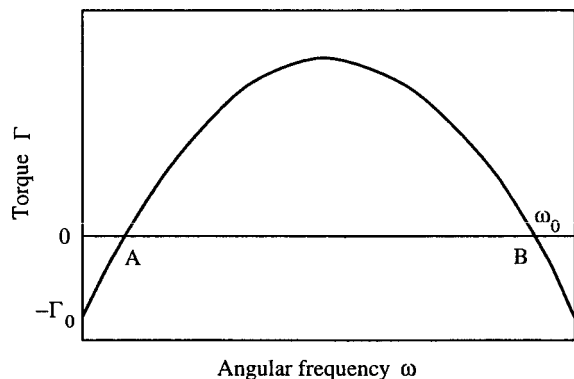


FIG. 8. Net accelerating torque  $\Gamma$  on the rotating slat as a function of rotation frequency  $\omega$ , for a fixed airspeed, according to the simple theory.  $\Gamma_0$  is the frictional torque. Note that the rotational speed must reach the point A if rotation is to be sustained; the rotation speed then increases to the steady value  $\omega_0$  at point B.

Finally, an expression must be derived for the torque  $\Gamma_3$  per unit length of slat driving the rotation. Again, this torque clearly varies periodically during the rotation, and the concern here is simply with its average value. A qualitative argument suggests that the mass flow per unit length intercepted by the slat per unit time is proportional to  $\rho W V$ , the imparted lateral speed due to slat rotation is proportional to  $W\omega$ , and the resultant moment is further proportional to  $W$ . This leads to the result, also supported by dimensional analysis, that

$$\Gamma_3 \approx \gamma \rho W^3 \omega V, \quad (7)$$

where  $\gamma$  is another nondimensional constant.

The complete first-order expression for the average torque per unit length acting on the slat is therefore

$$\Gamma = -\alpha \rho W^4 \omega^2 - (\beta + \beta') \rho W r V^2 - \Gamma_0 + \gamma \rho W^3 \omega V. \quad (8)$$

If this expression for  $\Gamma$  is plotted as a function of  $\omega$  for a fixed value of  $V$ , then it has the form shown in Fig. 8. Rotation can be maintained only over a limited range of angular velocity, explaining why the slat has to be set into rotation artificially and will not rotate spontaneously from rest. For angular velocities above the threshold A, the nett torque  $\Gamma$  is positive and the slat rotation speed increases until it comes to a steady state with rotation velocity  $\omega_0$  at the point B.

If the slat is to maintain its rotation, then it is clearly necessary that the rotation speed  $\omega_0$  for which  $\Gamma=0$  should be a real quantity—a statement equivalent to the requirement that the maximum value of  $\Gamma$  should be positive. Examination of the expression (8) shows that it is quadratic in  $\omega$  and that the condition  $\Gamma=0$  is met when

$$\frac{W\omega}{V} = \left( \frac{\gamma}{2\alpha} - \frac{\beta' r V}{2\alpha W^2} \right) \pm \left[ \left( \frac{\gamma}{2\alpha} - \frac{\beta' r V}{2\alpha W^2} \right)^2 - \frac{\beta r}{\alpha W} - \frac{\Gamma_0}{\alpha \rho W^2 V^2} \right]^{1/2}. \quad (9)$$

If this quantity is to be real, then the expression in square brackets must be positive, and this implies at least a minimum value for the airspeed  $V$  and at least a minimum value for the slat width  $W$ , both of these critical values depending

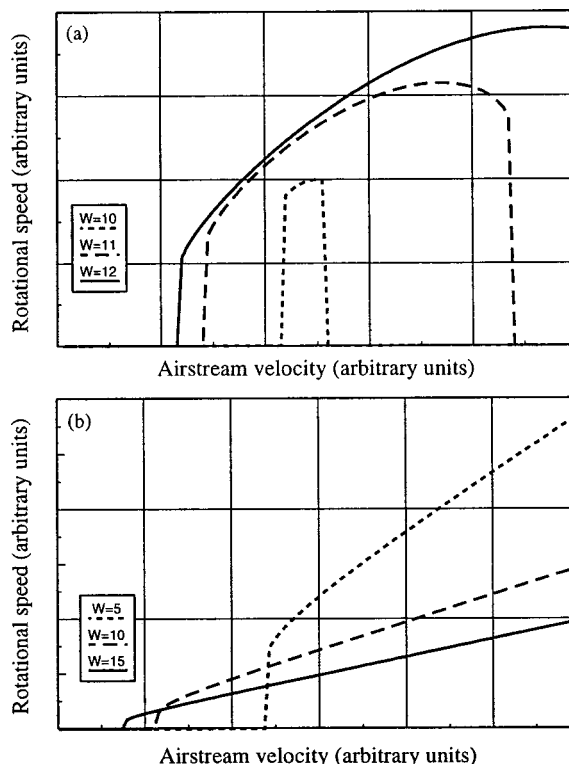


FIG. 9. (a) Predicted variation of steady rotational speed  $\omega_0$  with airspeed  $V$ , as given by Eq. (9), for a slat of width  $W$  with viscous torque in its bearings. (b) The same prediction for a slat with only static bearing torque  $\Gamma_0$ .

upon the bearing coefficients  $\Gamma_0$ ,  $\beta$  and  $\beta'$ . If these conditions are satisfied, then the steady rotational speed  $\omega_0$  of the slat will be given by (9) with the positive sign chosen.

The predictions of this theory are most easily seen by considering a numerical example. For this purpose we choose  $\alpha = \beta = \beta' = \gamma = 1$ ,  $\Gamma_0 = 1$ ,  $r = 1$ , and  $\rho = 1$  for simplicity. The results of the calculations are displayed in Fig. 9(a), which shows that, for a given slat width  $W$ , the rotation can be maintained only above a threshold airspeed determined by the frictional coefficients. There is also a maximum airspeed above which rotation ceases, and the airspeed region within which rotation can be maintained decreases in extent as the slat width  $W$  is reduced. Within this allowed region, the rotation speed tends to saturate and then decrease as the airspeed is increased, and the steady rotation speed for a given airspeed increases slowly with increasing slat width. All these predictions of the theory are in general qualitative agreement with the experimental wind-tunnel findings discussed in Sec. III, as can be seen by comparing Figs. 7 and 9(a).

In contrast, if the only bearing torque is a small constant value  $\Gamma_0$ , then once again this leads to threshold behavior, as shown in Fig. 9(b), but the rotational speed  $\omega$  of the slat then increases quasi-linearly with airspeed, and no upper limit is predicted. The rotational speed is also predicted to decrease smoothly with increasing slat width, all in contrast with the predictions and experimental results for viscous bearing friction shown in Fig. 9(a).

When the theory is applied to the case of a free bull-roarer slat whirled on the end of a string, the picture is quite

different because of the lack of bearing friction. Clearly  $\beta = \beta' = 0$  and the static torque  $\Gamma_0$  depends upon the twisting of the string and thus the integral  $\int \omega dt$ . Neglecting  $\Gamma_0$  in (9), as is valid near the mid-period of a rotation, leads to the result

$$\omega_0 = \frac{\gamma V}{\alpha W} = \text{const} \times \frac{F}{W}. \quad (10)$$

This result is in qualitative agreement with the experimental results shown in Fig. 6 and Eq. (3). No upper or lower limit to operational airspeed is predicted, provided the supporting string introduces no axial torque.

As a final tentative deduction from this simple theory, we note that the average lift force normal to the airstream direction can be expected to behave very much like the torque  $\Gamma_3$  except for a factor of order  $W^{-1}$ . This means that the sign of this force depends upon the sign of the rotation  $\omega$ , which is in accord with the observed conical path swept out by the string of a bullroarer. The angle of the cone described by the string path depends upon the ratio between the mean lift force and the centrifugal force, the simple theory suggesting that this ratio, and thus the cone angle, should be nearly independent of arm rotation speed since both terms increase as  $V^2$ . Such a lift effect is, of course, well known in the case of a rotating cylinder, where a rigorous derivation is possible.<sup>4</sup> It is noted here just to show that the simple theory above is at least consistent with a more rigorous theory.

## V. NUMERICAL ANALYSIS

Recognizing that the analysis above is at best semiquantitative, the aerodynamics underlying the behavior of rotational aerophones was further investigated by a numerical evaluation of the forces and torques acting on a rotating slat using the computational fluid dynamics software package Fluent 5.2.<sup>6</sup> This analysis was carried out only for the case of a freely rotating slat with no frictional forces.

Since the unsteady flow around a rotating plate can be turbulent, the Reynolds-averaged Navier–Stokes transport equations were used to represent the mean flow quantities, while the Reynolds stresses were modeled using the standard  $k-\epsilon$  (turbulent kinetic energy–turbulent dissipation rate) turbulence model.<sup>7</sup> The computational domain was divided into two subdomains: a stationary wind-tunnel domain, and a rotating circular domain containing the slat. The two domains were created using an “unstructured quadrilateral grid,” as defined in the software, with a higher density of nodes in the mesh near the interface between the two domains. The computational domain comprised a total of 6568 nodes covering a physical domain of dimensions  $200 \times 500$  mm, the longer dimension being in the flow direction. The slat, with a width  $W$  of only 40 mm, was located close to the input end of the domain. The rotational motion of the domain containing the slat was modeled using a sliding mesh technique.<sup>6</sup>

Calculations were carried out for a selected airspeed in the wind-tunnel and a given rotational speed of the slat, using a second-order upwind finite difference scheme in space and a second-order implicit finite difference scheme in time. Calculations were iterated until the flow around the slat be-

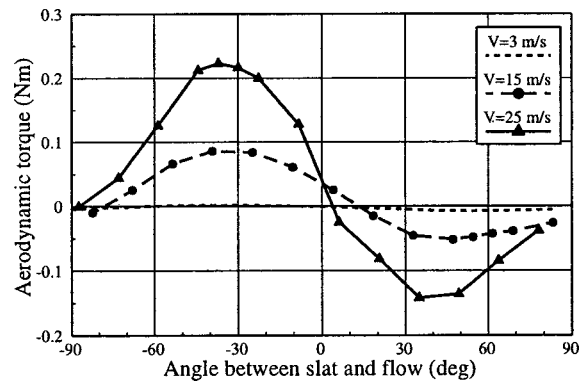


FIG. 10. Numerically calculated torque cycle on a slat of width 60 mm rotating at 50 revolutions per second in a stream with given speed. The second half of the cycle is identical. The mean accelerating torque  $\Gamma$  is the value of the signed area under the curve.

came periodic in time, as confirmed by observing the history of the computed force on the slat. The convergence was then checked by repeating one cycle of the calculation with a halved time step, and no significant difference was found.

Figure 10 shows the calculated torque on the rotating slat as a function of angle of orientation for given air flow speeds and a constant slat rotation speed. It is clear that there is a net steady torque on the slat, evaluated by taking the signed area between the curve and the axis, and that this net torque increases with air speed. Figure 11 displays the torque as a function of slat orientation for a constant air speed and given slat rotation speeds. Here it is clear that the net torque is positive for small rotation speeds, but becomes negative for large rotation speeds.

The results of the calculation can be plotted in a generalized nondimensional fashion as shown in Fig. 12, the plotted quantity being the torque coefficient  $C = 2\Gamma/\rho V^2$ , where  $\Gamma$  is the torque and  $V$  is the air speed. This is a more refined version of the semi-quantitative curve depicted previously in Fig. 8. There is a threshold value of the parameter  $\omega W/2V$ , where  $\omega$  is slat rotation speed,  $W$  is slat width, and  $V$  is air velocity, below which there is almost no net torque on the slat and so no induced rotation. With increasing values of the rotation speed  $\omega$ , the torque rises to a maximum and then becomes negative for parameter values above about 0.6. This calculation, of course, takes no account of bearing friction  $\Gamma_0$ , and the calculated torque must exceed  $\Gamma_0$  if rotation is to

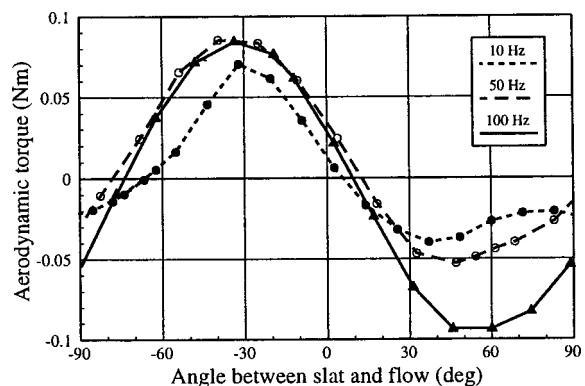


FIG. 11. Numerically calculated torque cycle on a slat of width 60 mm in a flow of  $15 \text{ m s}^{-1}$  for various rotation rates.

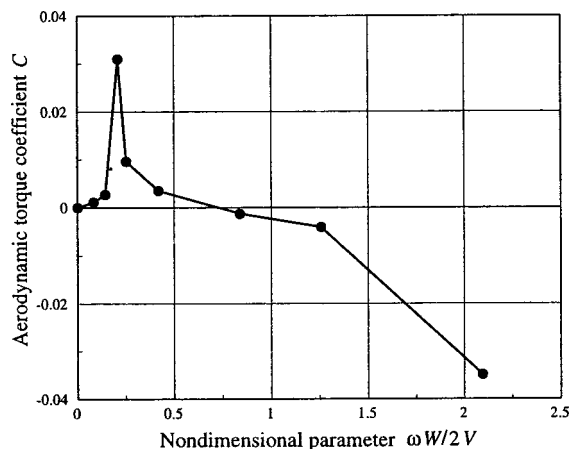


FIG. 12. Numerically calculated coefficient of aerodynamic torque as a function of the nondimensional parameter  $\omega W/2V$ , where  $\omega$  is rotation frequency,  $W$  is slat width, and  $V$  is airstream velocity.

be sustained. This suggests a parameter value in the range 0.3–0.5 for zero net torque, depending on the magnitude of the bearing friction. The steady rotation speed  $\omega_0$  attained by the slat will be that for which the net torque is zero, and hence about

$$\omega_0 \approx (0.6 \text{ to } 1.0)V/W. \quad (11)$$

Converting this to apply to the whirled bullroarer strip with string length of about 70 cm and a width  $W$  of about 60 mm gives  $\omega_0 \approx (0.4 \text{ to } 0.7)\Omega$ , where  $\Omega$  is the arm rotation rate. This conclusion is in good agreement with the measured result (2).

This numerical analysis, like the simple theory, does not reveal any upper limit to the air velocity  $V$  for which rotation will occur, and, as indicated in (11), suggests a slat rotation rate that increases linearly with airspeed. Both these findings are in agreement with measurements on the bullroarer (and incidentally with the simple theory of the previous section), confirming that the deviations from this behavior noted in wind-tunnel experiments can be attributed to bearing friction effects.

## VI. SOUND PRODUCTION

As discussed in Sec. II and shown in Fig. 4, the radiated sound spectrum is almost a simple amplitude-modulated sine wave with little harmonic development. This suggests that the basic sound-production process is simple and regular. A simple mechanism suggests itself, as discussed below, but first a simple dimensional analysis establishes the expected behavior.

The sound power  $P$  conceivably depends upon most of the variables of the situation, so that we write

$$P = \text{const} \times \rho^m M^n V^p W^q H^r, \quad (12)$$

where  $\rho$  is the air density,  $M = V/c$  is the Mach number,  $V$  is the translational velocity of the slat,  $W$  is its width, and  $H$  its length. Equating dimensions leads to the conclusion that  $m = 1$ ,  $p = 3$ , and  $q + r = 2$ , but we expect from the fact that the source dimensions are small compared with the sound wavelength that  $r = 2$ , so that  $q = 0$ . The power  $n$  of the nondimen-

sional Mach number  $M$  is undetermined, but we expect it to be non-negative. Indeed the dependence on  $M$  could well be more complicated than the simple power-law assumed. It can therefore be tentatively concluded that the radiated sound power is independent of the slat width  $W$  but varies as

$$P = \text{const} \times H^2 V^{3+n}, \quad (13)$$

where  $n \geq 0$ . This agrees with the experimental result (4) if  $n \approx 2.4 \pm 1$ .

In considering the sound-generation mechanism, it can be seen that the rotating slat moving through the still air clearly creates pressure and flow influences that have something of the character of a rotating and oscillating dipole source, with the positive pole of the dipole always directed upstream and having its maximum value when the slat is broadside on to its motion through the air. There are almost certainly quadrupole components as well, but these can be ignored to a first approximation because the power radiated by a macroscopic quadrupole is less than that from a dipole of the same monopole strength and source spacing  $W$  by a factor  $(\omega W/c)^2$ , which is of order  $10^{-2}$  in the present case.

The magnitude of each monopole flow source in the dipole is approximately  $HWV$  or  $HWL\Omega$ , where  $H$  is the length of the slat and  $L$  is the length of the string. The separation between the two sources is approximately  $W$ , so the dipole magnitude is about  $\mu \approx HW^2L\Omega$  and its acoustic frequency is  $\omega_s = 2\omega \approx 3L\Omega/W$  by (2). The acoustic power radiated by such a dipole source is<sup>5</sup>

$$P = \frac{\omega_s^4 \rho \mu^2}{24\pi c^3}, \quad (14)$$

where  $c$  is the speed of sound. Inserting expressions for  $\mu$  and  $\omega_s$  gives

$$P \approx \frac{3\rho H^2 L^6 \Omega^6}{c^3} = \frac{3\rho H^2 V^6}{c^3}. \quad (15)$$

This result, which predicts that sound power is proportional to  $\Omega^6$ , with no dependence on  $W$ , is in good agreement with the experimental result (4). Insertion of numerical values for the parameters of the slats used in the outdoor experiment gives a radiated power of order 1 mW, again in good agreement with measurements.

A related approach to the problem that has been well studied is the generation of sound by vortex shedding from a cylinder.<sup>8–10</sup> There are, of course, significant differences, in that vortex shedding in the cylinder case is correlated along its axis only by aerodynamic influences, giving a limited coherence length, while for a rotating slat coherence is enforced along its whole length by the slat rotation. Despite these differences, the cylinder case provides some guidance to the present problem. In particular, the frequency  $f = \omega/2\pi$  of vortex shedding derived from equation (11.3.28) of Morse and Ingard or (3.1.11) of Howe is approximately  $0.2V/d$ , where  $d$  is the cylinder diameter, this result agreeing almost exactly with the experimental result (3) for the rotating slat.

If the axial correlation length for vortex shedding is  $\Delta$ , then the radiated power per length  $\Delta$  is given by equation (11.3.30) of Morse and Ingard which, in simplified form, is

$$P(\Delta) \approx 0.005 \rho V^3 \Delta^2 M^3, \quad (16)$$

where  $M$  is the Mach number  $V/c$ . If  $\Delta$  is much less than the cylinder length  $H$ , then there are  $H/\Delta$  such sections along the cylinder and, since their phases are incoherent, their powers simply add, so that the total power radiated by the cylinder is given by (16) with  $\Delta^2$  replaced by  $H\Delta$ . This result is the same, except for a minor numerical multiplier, as that given by equation (3.1.13) of Howe,<sup>10</sup> which gives radiated intensity, including a directional factor  $\cos^2\theta$ .

For a rotating slat, however, the rotation ensures perfect correlation for aerodynamic behavior along the whole slat length  $H$ , so that  $\Delta$  should be replaced by the slat length  $H$ , provided this is much less than the sound wavelength. Once again there is no dependence of radiated power on the slat width  $W$ , and the power is proportional to  $H^2V^6$  as for the dipole model. There is, however, a great difference in the magnitude of the radiated power, that measured for the rotating slat being more than ten times the value calculated for an equivalent cylinder, even if coherence is assumed. A treatment related more directly to the slat geometry and including rotation could be expected to yield a higher power. The model underlying the aerodynamic generation of sound is, in fact, a refined version of the oscillating dipole model, so that the two are perhaps closely equivalent once the geometrical differences are taken into account.

The directionality of the sound radiation also requires some comment. In each of the explicit models discussed, the radiated sound is directed preferentially along the local direction of motion, which would be in the plane of rotation of the string if that motion were indeed planar. Because the dipole rotates as well as oscillating in sign, the radiation pattern is, however, much broader than for a simple dipole, and the conical form of the string path further broadens this distribution. There may also be some monopole component to the source, which would give a uniform angular distribution of the radiation. Taking these complications into account, it is not surprising that the radiation pattern is approximately uniform to within the modest accuracy of the experimental measurements.

## VII. DISCUSSION

The aim of this analysis has been to illuminate the behavior of rotational aerophones of the bullroarer family. This has been achieved in part. The analysis and simplified experiment shows that rotation can occur only above a certain airspeed that is determined by the frictional torque of the bearings. In the case of a bullroarer there are no bearings but rather a string that is progressively twisted by the rotation of the slat, the resisting torque thus increasing steadily with time until it is adequate to stop the rotational motion. The

torque then acts to accelerate rotation in the opposite sense, and the motion repeats itself. The period of this reversal, as judged by the sense of the cone described by the string or by the long-term behavior of sound level, is several seconds, though this is determined by the length and thickness of the string. The sound also pulsates at the arm rotation frequency and at twice that frequency, and the origin of these pulsations can be identified as the uneven rotational speed of the slat caused by elliptical arm motion.

Sound production is most easily visualized as the creation of an oscillating dipole across the slat as it rotates. Although such a dipole perturbs the downstream flow and generates a wake of vortices, the radiation from these is of relatively minor importance. A detailed treatment should, of course, include consideration of the aerodynamics of the wake, but largely in order to quantify more exactly the behavior of the attached dipole.

The behavior of rotational aerophones is much more complex to understand than is that of most other aerophones, because this behavior depends on aerodynamics and not on simple quasi-static pressure forces. The experiments and analysis detailed here do not by any means exhaust the possible study, but do provide an outline of the major phenomena and their likely explanation.

As a byproduct of the study, certain experimental problems associated with the apparently much simpler and better controlled environments provided by wind-tunnels and by anechoic rooms were identified and explained.

## ACKNOWLEDGMENTS

This study was supported by a grant from the Australian Research Council. The authors are grateful to the Associate Editor (Michael Howe) for pointing out an error in the original draft of the article.

<sup>1</sup>S. Marcuse, *A Survey of Musical Instruments* (Harper & Row, New York, 1975), pp. 549–550.

<sup>2</sup>N. H. Fletcher, “The didjeridu (didgeridoo),” *Acoustics Australia* **24**, 11–15 (1996).

<sup>3</sup>J. Antill, Ballet Suite “Corroboree,” Australian Broadcasting Commission (now Corporation), first British performance 1946.

<sup>4</sup>B. R. Munson, D. F. Young, and T. H. Okiishi, *Fundamentals of Fluid Mechanics* (Wiley, New York, 1998).

<sup>5</sup>N. H. Fletcher and T. D. Rossing, *The Physics of Musical Instruments*, 2nd ed. (Springer-Verlag, New York, 1998), pp. 172–174.

<sup>6</sup>*FLUENT 5 User's Guide* (Fluent Inc., Lebanon, NH, 1998).

<sup>7</sup>B. E. Launder and D. B. Spalding, *Lectures on Mathematical Models of Turbulence* (Academic, London, 1972).

<sup>8</sup>R. D. Blevins, “Review of sound induced by vortex shedding from cylinders,” *J. Sound Vib.* **92**, 455–470 (1984).

<sup>9</sup>P. M. Morse and K. U. Ingard, *Theoretical Acoustics* (McGraw-Hill, New York, 1968), pp. 717–777.

<sup>10</sup>M. S. Howe, *Acoustics of Fluid-Structure Interactions* (Cambridge U.P., Cambridge, 1998), Sec. 3.1.